Nanoscale Horizons

ROYAL SOCIETY OF CHEMISTRY

COMMUNICATION

View Article Online
View Journal | View Issue

Cite this: *Nanoscale Horiz.*, 2025, **10**, 3351

Received 12th May 2025,
Accepted 11th September 2025

DOI: 10.1039/d5nh00332f

rsc.li/nanoscale-horizons

Boron atom incorporation into metal nanoparticles

Jie Zhao,† Fernando Buendia-Zamudio † and Sergey M. Kozlov *

Boron can become unintentionally incorporated into transition metals during the reduction of metal salts with borohydride. The presence of boron at the surfaces of transition metals (TMs) such as Pd and Pt is known to significantly influence their catalytic properties. In this study, we employ density functional (DFT) calculations to investigate the thermodynamics and kinetics of boron incorporation into ~1.5 nm particles and extended (111) surfaces of fcc-Co, Rh, Ir, Ni, Pd, Pt, Cu, Ag, Au, and Al. Our results reveal that boron exhibits high thermodynamic stability in interstitial subsurface sites on (111) surfaces and nanoparticles of Rh, Pt, and Pd. Unlike extended surfaces, metal nanoparticles (NPs) can also stabilize boron within the coordination environment of surface metal atoms, with such sites being particularly stable in Rh, Ir, and Ni nanoparticles. Furthermore, the energy barriers for B migration at NP edge sites from the surface to subsurface decrease to <0.5 eV (for all metals except Ir), and the migration barrier for boron incorporation into the in-surface sites is lower than 0.2 eV. Notably, B incorporation induces a shift in the d-band center of adjacent metal atoms, which indicates its pronounced impact on the catalytic activity of transition metals.

New concepts

Transition metal nanoparticles of Pt, Pd, Rh, Ir, and Ni are calculated to incorporate boron atoms between the surface atoms into "in-surface" sites, which is a concept not observed in single-crystal surfaces. Moreover, the metal nanostructuring reduces the barrier for the migration of boron atoms from the surface to the highly stable in-surface and subsurface sites.

Introduction

Enhancing the performance of transition metal catalysts is crucial for the development of new processes in the chemical industry. Common strategies to enhance the catalytic performance of transition metals include elemental promotion, alloying, and engineering nanoparticle–support interactions.[1,2] Notably, some papers report on the critical role of small main-group atoms such as H,[3,4] B,[5] C,[6] and N[7] incorporated into transition metal catalysts on the electronic structure and activity of the latter.[8] The unintentional incorporation of light elements into TMs can occur during catalyst preparation or upon exposure to reaction conditions, potentially leading to uncontrolled effects on the catalytic activity.

For example, boron incorporation into metal nanoparticles (NPs) has been achieved using precursors such as boric acid[9] and diborane.[10] Indeed, many transition metals as well as Al[11] form strong bonds with boron atoms, resulting in the formation of metal borides, which exhibit a wide range of applications due to their exceptional mechanical[12] and catalytic properties.[13] For instance, nickel boride is widely used as a catalyst for reducing unsaturated hydrocarbons.[14] Moreover, the incorporation of low concentrations of boron atoms into TMs such as Co, Ni, Pd, and Pt has been reported in multiple studies.[14–18]

In particular, introducing boron enhances the stability of Pt and Pd catalysts by inhibiting the sintering of nanoparticles on metal oxide supports.[18–20] Additionally, boron doping was shown to enhance the catalytic activity of Pd supported on carbon black in the formic acid electro-oxidation reaction.[15,21] For example, Chan *et al.*[22] reported that boron residing in interstitial lattice sites of Pd nanoparticles improves the selectivity of the alkyne hydrogenation. A recent study on propane dehydrogenation over Pt/Al_2O_3 found that boron treatment alters the selectivity of the catalyst.[19] Other studies suggest that boron incorporation into supported Co NPs enhances CH_4 and CO_2 activation by stabilizing boron in the interstitial sites of fcc-Co(100) facets.[17] Similarly, Xu *et al.*[18] found that the addition of 1.0 wt% boron to Ni catalysts during methane steam reforming significantly improves the catalytic stability, reducing the deactivation rate by a factor of 3 and lowering carbon deposition by 80%. Sargent *et al.*[23] demonstrated that boron-doped copper enables tuning of the Cu^+/Cu^0 ratio and enhances

Department of Chemical and Biomolecular Engineering, Faculty of Engineering, National University of Singapore, 10 Kent Ridge Crescent, 119260, Singapore.
E-mail: sergey.kozlov@nus.edu.sg
† These authors contributed equally.

the C_2 product generation in electrochemical CO_2 reduction. Among coinage metals, the potential formation of subsurface boron has been suggested computationally only in Cu.[24] Additionally, Wang *et al.*[25] found, using DFT calculations, that the incorporation of dispersed boron atoms in Cu-based electrocatalysts significantly improves the selectivity of the CO_2 hydrogenation to ethanol. This enhancement arises from the B dopant acting as a charge transfer mediator, stabilizing key reaction intermediates and altering reaction pathways, ultimately facilitating C–C coupling to form ethanol.

However, the limited availability of unambiguous experimental characterization of B-treated transition metal catalysts has hindered a deeper exploration of the effect of B incorporation on the activity of transition metal catalysts. In particular, it remains unclear which metals preferentially form surface borides and how boron incorporation influences the geometric and electronic structure of the host metals.

To address these questions, we conducted a comprehensive thermodynamic and kinetic analysis of boron incorporation in NPs and (111) slabs of metals with face-centered cubic (fcc) crystal structures using statistical thermodynamics and transition state theory. Specifically, we examined group 9 (fcc-Co, Rh, Ir), group 10 (Ni, Pd, Pt), group 11 (Cu, Ag, Au), and Al. Our study investigates the adsorption and absorption behavior of a single boron atom on all possible surface, subsurface, and interstitial sites of metal (111) slabs as well as 140-atom NPs ($\sim$1.5 nm) under varying thermodynamic conditions using DFT calculations. The nanoparticle shape was chosen as truncated octahedral because this morphology is commonly observed experimentally[26] and allows direct comparison of the calculated properties with those of the (111) slab.

Results and discussion

The first step towards understanding boron incorporation in transition metals is to systematically examine its binding to all possible sites. Fig. 1 illustrates the fcc and hcp sites for a single boron atom adsorption on a metal surface, as well as octahedral subsurface sites (oss) and tetrahedral subsurface sites below hcp and top sites on the surface (tss and tss′, respectively). The DFT binding energy and Gibbs energy (relative to gas-phase B_2H_6) of the most stable configurations for boron on the NPs are shown in Fig. S1 and Fig. 2, respectively (more details are in the SI, Tables S1–S4). Please note that our tests show that the values calculated on the employed M_{140} models may differ by up to 0.08 eV from the respective values calculated on bigger M_{225} models (Table S3). Such modest dependence of the calculated results on the nanoparticle size implies the high transferability of the obtained results to NPs of various sizes, including those common in experimental studies and catalytic applications.

The binding energy of B is calculated to be negative on threefold hollow sites of Pt(111) and hcp sites of Ir(111), whereas on other metals, boron is unstable on surface sites. In general, boron subsurface absorption is energetically preferred over

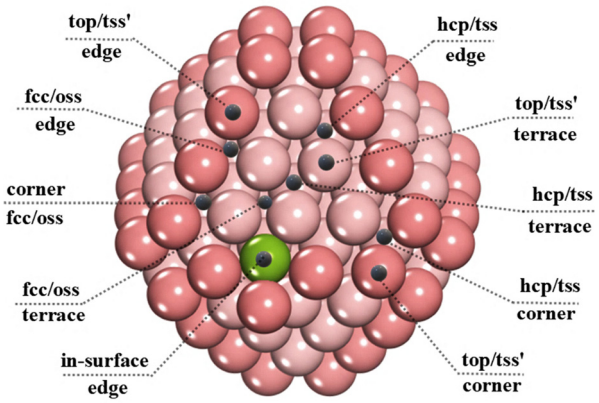

Fig. 1 Distinct surface/subsurface adsorption sites on {111} terraces, edges, and corners of M_{140} nanoparticles. The boron atom is marked as a green sphere; edge atoms are coloured with a darker shade.

surface adsorption among all metals except Ir. For other metals, the most stable oss subsurface sites exhibit $\sim$0.3, $\sim$0.5, and $\sim$0.7 eV stronger binding energies of B compared to the most stable adsorption sites on the respective metals from groups 9, 10, and 11, respectively.

The boron incorporation process into metal NPs could involve various sites due to the presence of metal atoms with different coordination numbers (for example, on corners and edges). The binding of B atoms to terraces of Pd NPs is exothermic due to their somewhat stronger adsorption strength compared to Pd(111). In turn, corner atoms on Rh and Ir NPs adsorb B atoms notably stronger than {111} NP terraces or (111) surfaces of the respective metals, which makes binding of surface B to corner Rh atoms exothermic. Finally, B atoms

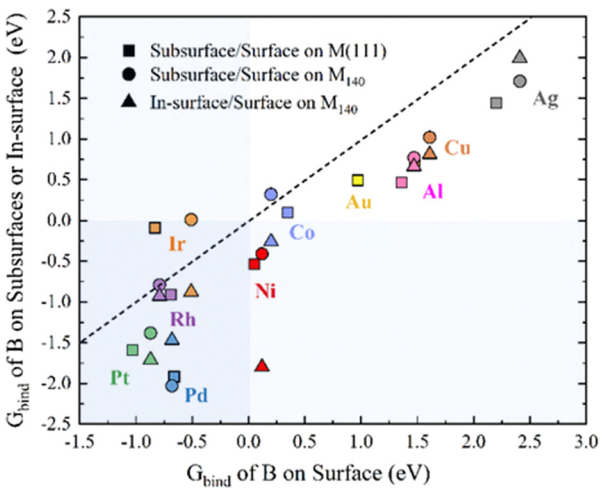

Fig. 2 Gibbs binding energies of the B atom at the most stable adsorption, "in-surface", and subsurface positions on the M(111) slab and NPs calculated at 298 K. Co is displayed as lavender blue, Rh – purple, Ir – orange, Ni – red, Pd – dark blue, Pt – green, Cu – brown, Ag – grey, Au – yellow, and Al – pink. The line ($y = x$) represents equal binding energies between the surface and subsurface or "in-surface" sites. The shaded area highlights the region with negative (*i.e.* exothermic) G_{bind} for adsorption or absorption of boron.

exhibit weaker binding energy on the surface of Co, Cu, Ag, and Al NPs compared to their (111) slabs. In contrast, the effect of nanostructuring is less significant for Ni and Pt. However, many adsorption sites are not locally stable for B atoms on metal nanoparticles because geometry optimization moves these B atoms in-between the surface metal atoms to a new type of site that we call ''in-surface'' (Fig. S2). These new sites become the most stable sites for B on all studied metal nanoparticles except Pd, Pt, and Ag. In particular, B binds stronger in the ''in-surface'' sites on Ni nanoparticles, with more than 1 eV higher stability than other sites. Importantly, these sites are not locally stable for B on (111) slabs of the considered metals except Al, where these sites are relatively unstable (Table S1).

In turn, metal nanoparticles exhibit weaker B binding energies in all subsurface sites of fcc-Co, Ir, Ni, Cu, Ag, Au, and Al compared to the respective (111) surfaces (Fig. S3). In contrast, the stability of B is increased when it is located in the oss terrace subsurface sites of Rh, Pd, and Pt nanoparticles compared to respective (111) slabs. In contrast, the binding energy of B to subsurface oss sites on Ag NPs remains positive despite their highest stability among all sites. The B atoms are calculated to be locally unstable in many of the subsurface sites in the considered NPs because they move from them to adjacent ''in-surface'' sites during geometry optimization. The impact of boron on the geometric structure of metal surfaces is a question of interest due to its role in the formation and breaking of metal–metal bonds. To explore this effect, the displacement of the three neighbouring metal atoms and the final height of the boron atom above the metal surface were analyzed (eqn (S1), (S2) and Fig. S4, S5). The boron absorbed on Au and Al (111) generates the largest distortion and the closest boron-surface distance among all examined metals. In general, the distortion generated by the B adsorption on the edge sites of the NPs is more pronounced than that of the (111) NP terrace. However, once B migrates to the subsurface, the level of distortion becomes comparable to that observed on the (111) surface. Conversely, when B is adsorbed at a terrace site on the NPs, the distortion is greater than that observed on the (111) surfaces. The most substantial distortion occurs when the B atom is positioned at the ''in-surface'' of the NP, as it generates the breaking of M–M bonds. The presence of B at this ''in-surface'' site could play an essential role in the catalytic properties of the new system, as it introduces a novel active site with distinct characteristics compared to the host metal atoms in the NP.

To analyse the contribution of structural displacements to the stability of B atoms in the metals, we decompose their binding energies into electronic interaction energy and distortion energy of the metal substrate (eqn S3–S5). The distortion energies are quite small when B atoms are adsorbed on metal slabs or nanoparticles and seem to become higher for heavier transition metals (Fig. S6, S7). In turn, the distortion of the metal substrate is much higher when B is located in subsurface sites and correlates with the group of the metal atoms in the periodic table. Surprisingly, the distortion of metal NPs is similar for the B location at the subsurface and at the surface positions. In general, the results suggest that increasing the coordination of the B atom enhances the interaction energy but also induces larger geometric distortion, which imposes a penalty on the system's stability. However, this penalty is smaller than the gain in interaction energy, resulting in higher stability of the subsurface and ''in-surface'' sites for most metals. This finding is particularly important for NPs, where the most distorted ''in-surface'' sites emerge as the most stable configurations for certain metals. Please note that the calculated binding energies of B atoms only roughly correlate with the size of the metal atoms composing the NP, although previous studies suggested that structures with five-fold symmetries may be stabilized at certain degrees of size mismatch.[27]

Another question is whether the subsurface or ''in-surface'' boron atoms can form in metal substrates during a typical synthesis procedure. To address this, we evaluate the Gibbs free energy of a typical source of B in the experiment, namely B_2H_6, decomposition into H_2 and B atoms under different thermodynamic conditions (eqn (S6), S7 and Tables S5, S6). We focus our analysis on B_2H_6 because its gas phase under ambient conditions makes it more reactive than other boron precursors like H_3BO_3. For the boron atom interacting with (111) slabs, all the surface and subsurface sites of Pd and Pt are more stable relative to the boron precursor (B_2H_6) in the gas phase at standard temperature and pressure (Fig. 2). In turn, for Ni, G_{bind} is negative only in the subsurface of (111) slabs and NP. In contrast, group 11 elements and Al do not have any site where the B adsorption or absorption possesses a negative G_{bind} value. Furthermore, Ir and Rh stabilize B on the surface of single crystals or ''in-surface'' of NPs, whereas fcc-Co stabilizes B slightly only on the ''in-surface'' sites of the NP models (Table S6). The incorporation of B in cobalt nanoparticles and its effect on the catalyst activity in the methane dry reforming reaction have been described by Takanabe *et al.* in previous studies.[17]

The higher stability of subsurface and ''in-surface'' sites compared to those of the surface sites raises the question of the kinetic feasibility of boron migration (Fig. 3 and Tables S7, S8). For Rh and Ir (111) slabs, the barriers for boron migration from surface fcc sites to subsurface oss sites ($G_b > 1.1$ eV) are the highest of all the metals studied, making these transition processes unlikely even at relatively high temperatures. In contrast, the fcc-Co NP and Pd group exhibit lower energy barriers for boron boring from fcc to oss sites on the (111) slab, ranging from 0.37 to 0.84 eV. The lowest barriers on the (111) surfaces are observed for Cu, Ag, and Au in group 11, with values of 0.47, 0.29, and 0.22 eV, respectively. Moreover, the barrier for boron incorporation into Al NPs is below the thermal energy threshold (k_BT). We also studied B migration from hcp to tss sites for metals, where the latter sites are stable for B (Ir, Pd, Pt, and Au). The results show that the activation barriers for B migration from hcp to tss sites are similar to the barriers for the migration from fcc to oss sites on all considered metals. Please note that such low migration barriers do not undermine the stability of subsurface boron. For example, our molecular dynamics simulations confirm that B in a subsurface oss site in

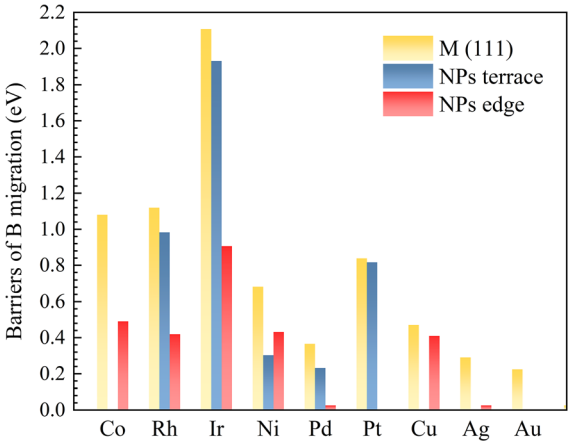

Fig. 3 Gibbs free energies of the barrier for the migration process of a boron atom from fcc to oss sites on the metal (111) surface and M_{140} at 298 K.

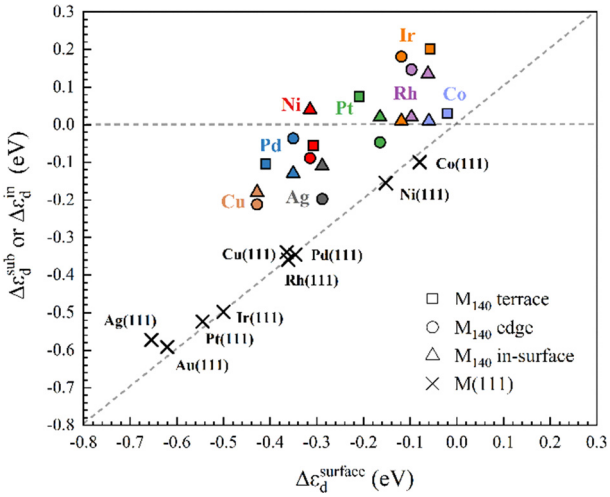

Fig. 4 Relationship between the d-band center shift on adjacent metal atoms to B in surface fcc ($\Delta\varepsilon_d^{sur}$) and subsurface oss ($\Delta\varepsilon_d^{sub}$) sites, as well as in-surface ($\Delta\varepsilon_d^{in}$) sites on M(111) surfaces and NPs. Co is displayed as lavender blue, Rh – purple, Ir – orange, Ni – red, Pd – blue, Pt – green, Cu – brown, Ag – grey, Au – yellow, and Al – pink. The diagonal line ($y = x$) represents equivalent values in the d-band shift for surface and subsurface positions. The horizontal line ($y = 0$) represents a zero shift of the B-doped metal compared to the pristine material.

Pd nanoparticles is stable for, at least, 10 ps at 300 K. However, the Gibbs barrier for its migration to the surface is around 1.4 eV (Fig. S9). The stability of boron located at the tss site of the Pd NP, where the barrier to migrate to the surface is only 0.45 eV, was also determined using a similar MD simulation. In this case, the B atom preferred to diffuse to the neighbouring oss site after 1.5 ps.

Interestingly, the energy barriers for B incorporation decreased significantly at the NP edges relative to the barriers on M(111) slabs. For fcc edge sites, nanostructuring of Rh and Ir reduced the barriers of B migration by 0.70 and 1.20 eV, whereas on Ni and Pd the nanostructuring reduced these barriers to 0.43 and 0.03 eV, respectively (Fig. 3). The B transition from fcc to oss sites on terrace nanoparticle positions presents only minor variations in their barriers compared to the (111) surfaces because of similar coordination numbers of terrace metal atoms. On the other hand, the B transition from hcp to tss sites on terrace nanoparticle positions exhibits a great reduction for Rh and Pd compared with the other sites. Notably, the exceptionally low barrier for B migration on Pd NPs is of particular interest, as the stability of B at oss sites is the highest among all metals. Additionally, the absence of stable surface sites for B adsorption on Al and Au NPs could suggest that B migration in the subsurface is spontaneous on these metal NPs. In turn, most metals present barrierless B migration from the surface into "in-surface" sites. The only exceptions are fcc-Co, Ni, Rh, and Ir with barriers below 0.2 eV. These results indicate that the "in-surface" sites are readily accessible across all metals. Overall, the B migration barriers from the surface to subsurface of the NPs decrease in all cases compared with the metal (111) surfaces; the barriers of group 9 (Co, Rh, Ir) are still, on average, higher than those of group 10 (Ni, Pd, Pt), and group 11 (Cu, Ag, Au). Finally, the surface/"in-surface" migration exhibits barriers below 0.2 eV due to the highest stability of the latter sites on all metals except Pd and Pt.

The incorporation of B modifies the electronic structure of adjacent metal atoms (Fig. 4 and Table S9), which is crucial for their catalytic properties. For example, oss subsurface B bestows negative charge between 0.3 and 0.6 to the adjacent surface metal on (111) surfaces of Rh, Ir, Pd, and Pt. The charging of surface metals by B is amplified between −0.8 and −0.5 a.u. on Pd and Pt NPs. Similar charges between −0.55 and −0.4 a.u. are calculated on Rh and Ir atoms adjacent to "in-surface" B atoms in nanostructured metals, whereas no charge is found on Co and Ni atoms.

In turn, the d-band shift is the most pronounced for adsorbed B atoms, because subsurface and in-surface B atoms induce tensile strain in the metal substrate, which pushes the d-band in the opposite direction.[16] Thus, the subsurface B in (111) surfaces shifts the d-band centers, $\Delta\varepsilon_d$, of adjacent metal atoms to 0.3–0.5 eV towards more negative values, whereas these effects can be reduced almost to zero on metal nanoparticles.

Conclusions

Our comprehensive computational analysis of B binding to various sites on (111) surfaces and nanoparticles of fcc-Co, Rh, Ir, Ni, Pd, Pt, Cu, Ag, Au, and Al revealed that non-coinage transition metals can incorporate B. Namely, boron atoms are highly stable in the subsurface region of the (111) surfaces of Rh, Pd, and Pt. However, the activation energies for subsurface B formation in the (111) surfaces of fcc-Co, Rh, Ir, and Pt are above 0.8 eV, and only for Pd(111), this barrier is as low as 0.34 eV. Moreover, this barrier for B migration into the subsurface decreases below 0.2 eV on {111} terraces of the Pd NPs. The calculated barriers for boron incorporation are also below 0.5 eV at the NP edge sites, for all metals except Ir.

Interestingly, on Co, Rh, Ir, and Ni nanoparticles, B atoms have the highest stability at ''in-surface'' edge sites, where B is in the same plane as surface metal atoms. The activation barriers for B migration from surface to ''in-surface'' are calculated to be below 0.2 eV, which indicates a high rate of this process under exposure of the metal to B-containing compounds. Our analysis shows that the distortion of metal substrates is similar upon B incorporation into ''in-surface'' or subsurface sites, but much higher than the distortion by adsorbed B. At the same time, B dopants have low stability on nanostructured or single-crystalline Cu, Ag, Au, and Al, although the barriers for B migration between various sites on these metals are below 0.4 eV.

The incorporation of B can decrease the charges on adjacent metal atoms in Rh, Ir, Pd, and Pt by 0.3–0.8 a.u., and shift their d-band by up to 0.5 eV towards more negative energies. Hence, controlled or uncontrolled incorporation of B into subsurface or ''in-surface'' sites on non-coinage transition metals during catalyst synthesis could be expected to dramatically change their catalytic properties.

Author contributions

Jie Zhao performed the formal analysis, investigation, and visualization of the draft. Fernando Buendia-Zamudio contributed to the formal analysis, investigation, visualization, and writing – original draft. Sergey M. Kozlov contributed to the conceptualization, project administration, resources, writing – review, and editing.

Conflicts of interest

There are no conflicts to declare.

Data availability

The data supporting this article have been included as part of the SI. See DOI: **https://doi.org/10.1039/d5nh00332f**.

Acknowledgements

This work was supported by the National research Foundation under NRF fellowship NRFF13-2021-0126. Computational work was performed using resources of the National Supercomputing Centre, Singapore.

References

1 J. S. Yoo, Z.-J. Zhao, J. K. Nørskov and F. Studt, Effect of Boron Modifications of Palladium Catalysts for the Production of Hydrogen from Formic Acid, *ACS Catal.*, 2015, **5**(11), 6579–6586, DOI: **10.1021/acscatal.5b01497**.

2 K. M. Neyman and S. M. Kozlov, Quantifying Interactions on Interfaces between Metal Particles and Oxide Supports in Catalytic Nanomaterials, *NPG Asia Mater.*, 2022, **14**(1), 59, DOI: **10.1038/s41427-022-00405-4**.

3 J. Greeley and M. Mavrikakis, Surface and Subsurface Hydrogen: Adsorption Properties on Transition Metals and Near-Surface Alloys, *J. Phys. Chem. B*, 2005, **109**(8), 3460–3471, DOI: **10.1021/jp046540q**.

4 B. Lin, X. Wu, L. Xie, Y. Kang, H. Du, F. Kang, J. Li and L. Gan, Atomic Imaging of Subsurface Interstitial Hydrogen and Insights into Surface Reactivity of Palladium Hydrides, *Angew. Chem., Int. Ed.*, 2020, **59**(46), 20348–20352, DOI: **10.1002/anie.202006562**.

5 Z. Mao, C. Ding, X. Liu, Q. Zhang, X. Qin, H. Li, F. Yang, Q. Li, X.-G. Zhang, J. Zhang and W.-B. Cai, Interstitial B-Doping in Pt Lattice to Upgrade Oxygen Electroreduction Performance, *ACS Catal.*, 2022, **12**(15), 8848–8856, DOI: **10.1021/acscatal.2c01052**.

6 F. Viñes, C. Loschen, F. Illas and K. M. Neyman, Edge Sites as a Gate for Subsurface Carbon in Palladium Nanoparticles, *J. Catal.*, 2009, **266**(1), 59–63, DOI: **10.1016/j.jcat.2009.05.010**.

7 I. V. Yudanov, K. M. Neyman and N. Rösch, Density Functional Study of Pd Nanoparticles with Subsurface Impurities of Light Element Atoms, *Phys. Chem. Chem. Phys.*, 2004, **6**(1), 116–123, DOI: **10.1039/B311054K**.

8 T. Chen, C. Foo and S. C. Edman Tsang, Interstitial and Substitutional Light Elements in Transition Metals for Heterogeneous Catalysis, *Chem. Sci.*, 2021, **12**(2), 517–532, DOI: **10.1039/D0SC06496C**.

9 H.-X. Zhang, S.-H. Wang, K. Jiang, T. André and W.-B. Cai, In Situ Spectroscopic Investigation of CO Accumulation and Poisoning on Pd Black Surfaces in Concentrated HCOOH, *J. Power Sources*, 2012, **199**, 165–169.

10 K. Jiang, K. Xu, S. Zou and W.-B. Cai, B-Doped Pd Catalyst: Boosting Room-Temperature Hydrogen Production from Formic Acid–Formate Solutions, *J. Am. Chem. Soc.*, 2014, **136**(13), 4861–4864, DOI: **10.1021/ja5008917**.

11 X.-J. Feng and Y.-H. Luo, Structure and Stability of Al-Doped Boron Clusters by the Density-Functional Theory, *J. Phys. Chem. A*, 2007, **111**(12), 2420–2425.

12 G. Akopov, L. E. Pangilinan, R. Mohammadi and R. B. Kaner, Perspective: Superhard Metal Borides: A Look Forward, *APL Mater.*, 2018, **6**(7), 070901, DOI: **10.1063/1.5040763**.

13 Y. Yao, Z. Zhang and L. Jiao, Development Strategies in Transition Metal Borides for Electrochemical Water Splitting, *Energy Environ. Mater.*, 2022, **5**(2), 470–485, DOI: **10.1002/eem2.12198**.

14 C. A. Brown, Catalytic Hydrogenation. V. Reaction of Sodium Borohydride with Aqueous Nickel Salts. P-1 Nickel Boride, a Convenient, Highly Active Nickel Hydrogenation Catalyst, *J. Org. Chem.*, 1970, **35**(6), 1900–1904, DOI: **10.1021/jo00831a039**.

15 J.-Y. Wang, Y.-Y. Kang, H. Yang and W.-B. Cai, Boron-Doped Palladium Nanoparticles on Carbon Black as a Superior Catalyst for Formic Acid Electro-Oxidation, *J. Phys. Chem. C*, 2009, **113**(19), 8366–8372, DOI: **10.1021/jp900349g**.

16 H. Li, X. Qin, X.-G. Zhang, K. Jiang and W.-B. Cai, Boron-Doped Platinum-Group Metals in Electrocatalysis: A

Perspective, *ACS Catal.*, 2022, **12**(20), 12750–12764, DOI: 10.1021/acscatal.2c04358.

17 A. J. Al Abdulghani, J.-H. Park, S. M. Kozlov, D.-C. Kang, B. AlSabban, S. Pedireddy, A. Aguilar-Tapia, S. Ould-Chikh, J.-L. Hazemann and J.-M. Basset, *et al.*, Methane Dry Reforming on Supported Cobalt Nanoparticles Promoted by Boron, *J. Catal.*, 2020, **392**, 126–134.

18 J. Xu, L. Chen, K. Tan, A. Borgna and M. Saeys, Effect of Boron on the Stability of Ni Catalysts during Steam Methane Reforming, *J. Catal.*, 2009, **261**(2), 158–165, DOI: 10.1016/j.jcat.2008.11.007.

19 M. Aly, E. L. Fornero, A. R. Leon-Garzon, V. V. Galvita and M. Saeys, Effect of Boron Promotion on Coke Formation during Propane Dehydrogenation over Pt/γ-Al2O3 Catalysts, *ACS Catal.*, 2020, **10**(9), 5208–5216, DOI: 10.1021/acscatal.9b05548.

20 J. Li, J. Chen, Q. Wang, W.-B. Cai and S. Chen, Controllable Increase of Boron Content in B-Pd Interstitial Nanoalloy To Boost the Oxygen Reduction Activity of Palladium, *Chem. Mater.*, 2017, **29**(23), 10060–10067, DOI: 10.1021/acs.chemmater.7b03732.

21 H. Liu, M. Huang, W. Tao, L. Han, J. Zhang and Q. Zhao, A Palladium Catalyst Supported on Boron-Doped Porous Carbon for Efficient Dehydrogenation of Formic Acid, *Nanomaterials*, 2024, **14**(6), 549.

22 C. W. A. Chan, A. H. Mahadi, M. M.-J. Li, E. C. Corbos, C. Tang, G. Jones, W. C. H. Kuo, J. Cookson, C. M. Brown, P. T. Bishop and S. C. E. Tsang, Interstitial Modification of Palladium Nanoparticles with Boron Atoms as a Green Catalyst for Selective Hydrogenation, *Nat. Commun.*, 2014, **5**(1), 5787, DOI: 10.1038/ncomms6787.

23 Y. Zhou, F. Che, M. Liu, C. Zou, Z. Liang, P. De Luna, H. Yuan, J. Li, Z. Wang, H. Xie, H. Li, P. Chen, E. Bladt, R. Quintero-Bermudez, T.-K. Sham, S. Bals, J. Hofkens, D. Sinton, G. Chen and E. H. Sargent, Dopant-Induced Electron Localization Drives CO2 Reduction to C2 Hydrocarbons, *Nat. Chem.*, 2018, **10**(9), 974–980, DOI: 10.1038/s41557-018-0092-x.

24 Q. T. Trinh, A. Banerjee, Y. Yang and S. H. Mushrif, Sub-Surface Boron-Doped Copper for Methane Activation and Coupling: First-Principles Investigation of the Structure, Activity, and Selectivity of the Catalyst, *J. Phys. Chem. C*, 2017, **121**(2), 1099–1112, DOI: 10.1021/acs.jpcc.6b09236.

25 J.-S. Wang, G.-C. Zhao, Y.-Q. Qiu and C.-G. Liu, Strong Boron–Carbon Bonding Interaction Drives CO_2 Reduction to Ethanol over the Boron-Doped Cu(111) Surface: An Insight from the First-Principles Calculations, *J. Phys. Chem. C*, 2021, **125**(1), 572–582, DOI: 10.1021/acs.jpcc.0c09661.

26 Y. Xia, Y. Xiong, B. Lim and S. E. Skrabalak, Shape-Controlled Synthesis of Metal Nanocrystals: Simple Chemistry Meets Complex Physics?, *Angew. Chem., Int. Ed.*, 2009, **48**(1), 60–103.

27 N. Canestrari, D. Nelli and R. Ferrando, General Theory for Packing Icosahedral Shells into Multi-Component Aggregates, *Nat. Commun.*, 2025, **16**(1), 1655.

